CrossMark

Microstrip Resonators and Broadband Lines for X-band EPR Spectroscopy of Molecular Nanomagnets

Alberto Ghirri[1] · **Claudio Bonizzoni**[4] ·
Mattia Righi[2] · **Federico Fedele**[2] · **Grigore Timco**[3] ·
Richard Winpenny[3] · **Marco Affronte**[4]

Abstract We present a practical setup to perform continuous-wave X-band electron paramagnetic resonance spectroscopy by using planar microstrip lines and general purpose instrumentation. We fabricated Ag/alumina and Nb/sapphire microstrip resonators and transmission lines and compared their performance down to 2 K and under applied magnetic field. We used these devices to study single crystals of molecular Cr_3 nanomagnets. By means of X-band planar resonators we measured angle-dependent spectra at fixed frequency, while broadband transmission lines were used to measure continuous wave spectra with varying frequency in the range 2–25 GHz. The spectra acquired at low temperatures allowed to extract the essential parameters of the low-lying energy levels of Cr_3 and demonstrate that this method is particularly suitable to study small crystals of molecular nanomagnets.

1 Introduction

Electron paramagnetic resonance (EPR) is a powerful spectroscopic technique widely used in chemistry, physics and biology. Conventional spectrometers usually employ 3D cavities that are optimized for specific electromagnetic (e.m.) modes and transitions [1]. To date, a large variety of them has been developed for specific

✉ Alberto Ghirri
alberto.ghirri@nano.cnr.it

1   CNR-Istituto Nanoscienze, via Campi 213/a, 41125 Modena, Italy

2   Dipartimento di Scienze Fisiche, Informatiche e Matematiche, Università di Modena
    e Reggio E, via Campi 213/a, 41125 Modena, Italy

3   School of Chemistry and Photon Science Institute, The University of Manchester,
    Oxford Road, M13 9PL Manchester, UK

4   CNR-Istituto Nanoscienze and Dipartimento di Scienze Fisiche, Informatiche e Matematiche,
    Università di Modena e Reggio E, via Campi 213/a, 41125 Modena, Italy

applications, including high and multi-frequency, pulses, electron-nuclear double resonance, etc., as well as coherent manipulation of quantum states by means of sequences of pulses [2]. Planar resonator have been proposed as an alternative approach for magnetic resonance experiments and different geometries, including stripline [3], microstrip [4–8], coplanar [9–11] and microcoils [12–15] have been studied in detail. Similar resonators were also used for ferromagnetic resonance measurements [16–18] while superconducting analogs have been used in circuit-QED experiments with superconducting qubits and spin ensembles [19]. Microstrip and coplanar circuits find also widespread applications in telecommunications as filters or antennas. These devices are fabricated by microelectronic circuit technology, that allows flexibility of design and scalability. The peculiar characteristic of planar resonators is the possibility to perform on-chip EPR spectroscopy on miniaturized samples such as small crystals, nanostructures, films or metamaterials. The microwave field can be adapted to the size of the sample to obtain improved sensitivity, which can comparable, or even superior, to that of conventional spectrometers [12–15]. Another characteristic is their excellent conversion efficiency, which allows to generate strong microwave fields with reduced power and dissipation. Together with the small heat load, it allows microresonators to be installed in cryogenic refrigerators to carry out EPR spectroscopy at mK temperature [9].

In this paper, we describe a simple and flexible setup based on planar resonators installed in a commercial cryo-magnetic system. A vector network analyzer (VNA) is used for the detection of the EPR signal in the range 2–25 GHz. We have designed and fabricated different types of planar resonators and we have tested them on different kinds of molecular nanomagnets (crystals, powders and films). In particular, here we compare the results obtained by means of resistive Ag/alumina devices to superconducting Nb/sapphire resonators. The superconductor allows to suppress the resistive losses and to increase the quality factor. This, in turn, should result in an improved sensitivity of the device. Our results demonstrate that this techniques is well suited for the characterization and study of these materials. We focus on a set of measurements that have been carried out on molecular Cr_3 triangles. They are constituted by three Cr^{3+} ions, each one carrying spin 3/2, coupled by antiferromagnetic Heisenberg exchange that give rise to a doublet ground and first excited states well separated from the higher lying energy levels [20]. The performances and sensitivity of the fabricated microstrips are tested by measuring the same sample under different conditions.

2 Microstrip Fabrication and Test

Microstrip devices require a dielectric substrate and a double-side deposition of a conductive film. On the top side, a strip having well-defined dimensions is patterned by lithographic methods, while the bottom side is used as ground electrode. For a substrate with given thickness (t) and dielectric permeability (ϵ_r), the width of the strip (w) can be calculated by standard methods to obtain a nominal impedance of 50 Ω [21]. In our case, from ϵ_r (alumina) $= 9.9$ and $t = 0.63$ mm we obtained
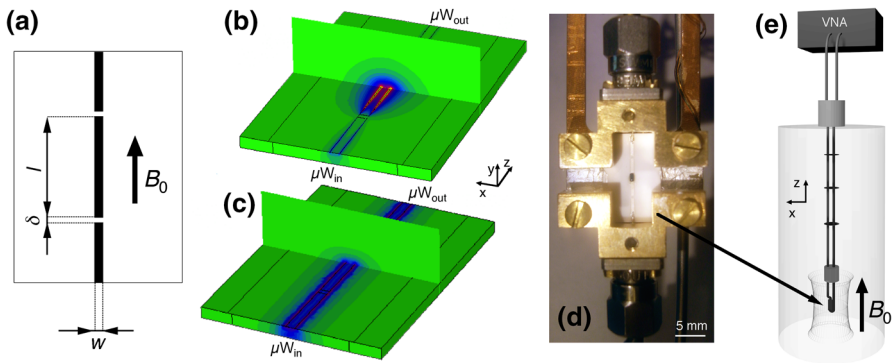
Fig. 1 **a** Schematic of the resonator. **b**, **c** Finite element simulation of the averaged distribution of $|\mathbf{B_1}|$, respectively, for **b** resonator and **c** broadband line. **d** Photograph of the Ag/alumina resonator installed in the metal box. The single crystal of Cr_3 is located at the center of the microstrip. **e** Drawing of the low-temperature setup

$w = 0.5$ mm (Fig. 1). The transmission of an e.m. wave through the microstrip takes place with a quasi-transverse mode, where the magnetic component $\mathbf{B_1}$ oscillates perpendicular to the central strip. In our setup the dc magnetic field $\mathbf{B_0}$ is applied parallel to the strip. This assures that we can perform perpendicular-mode EPR spectroscopy with the canonical selection rules [1].

Planar resonators can be easily realized by interrupting the microstrip line in two points through coupling gaps of width δ. The central strip of length l constitutes the $\lambda/2$ resonator (Fig. 1). In our case, $l = 6$ mm corresponds to a fundamental mode of frequency $v_0 = \frac{c}{2\sqrt{\epsilon_{eff}}(l+\Delta l)} \simeq 9.2$ GHz, where $c = 3 \times 10^8$ m/s, $\epsilon_{eff} = 6.4$ [21] and Δl is a correction factor to take into account the effect of the gap [3]. By increasing δ the resonating strip is progressively decoupled from the feedlines and the quality factor (Q) increases. On the other hand, the insertion loss (IL) increases as well. This limits the signal transmitted through the microstrip and also the magnitude of the microwave field ($\mathbf{B_1}$). We initially fabricated a test series of resonators to choose δ and we obtained that $\delta = 300$ μm was a satisfactory choice. To calculate the distribution of $\mathbf{B_1}$ we performed finite element e.m. simulations (CST Microwave Studio). As expected for a $\lambda/2$ resonator, Fig. 1b shows that an antinode of $|\mathbf{B_1}|$ is located at the center of the strip. The simulated maximum field ($|\mathbf{B_1}| \sim 10^{-4}$ T for an input power of 1 W) is in similar to other results reported in the literature [15]. For comparison, the simulation carried out for the microstrip transmission line (Fig. 1c) shows that the maximum value of $|\mathbf{B_1}|$ is ten times lower than the resonator. Besides the possibility to span on different frequencies, the broadband line is thus expected to have lower sensibility.

Different choices for dielectric and conductors are possible, yet we found good tradeoff by fabricating silver microstrips by one-step optical lithography (lift-off) on $14 \times 10 \times 0.63$ mm^3 alumina substrates ($\epsilon_r = 9.9$). 3-μm-thick Ag film was thermally evaporated and post-annealed in vacuum at 400 °C for 2 h. This thickness allows to exceed the skin depth of silver in this frequency range ($\simeq 0.7$ μm). Nb/sapphire resonators were fabricated by means of the same

lithographic mask used for the Ag/alumina resonator. Niobium films (thickness 350 nm) were deposited on sapphire (ϵ_r (sapphire) $= 11.5$) by sputtering (base pressure 10^{-6} mBar, growth rate 0.5 Å/s).

The microstrips were installed in a open box made of gold-plated brass (Fig. 1d) that defines the ground and shields the resonator from the environment. The bottom side of the chip is glued to the base by means of silver paint, the central strip is instead glued to the pins of the microwave launchers. The launcher connects pin and coaxial line through SMA connectors. Measurements were carried out in vacuum and down to $T = 2$ K in a commercial Quantum Design PPMS cryostat, by means of a dedicated insert wired with low thermal conductivity coaxial cables (Micro-Coax UT-085B-SS). These are thermalized at an intermediate stage to the sample chamber of the PPMS by means of contact fingers, and brought out of the cryostat, without interruptions, by means of o-ring sealed vacuum feedthroughs (Fig. 1e). The temperature is monitored by means of a calibrated ruthenium oxide thermometer mounted on the back of the microstrip box.

To characterize the frequency response of these devices, we measured the reflection (S_{11}) and transmission (S_{21}) scattering parameters by means of a Vector Network Analyzer (Agilent PNA 26.5 GHz). Figure 2 shows the comparison between the typical S_{11} and S_{21} spectra of the Ag/alumina and Nb/sapphire resonators. In both cases the presence of the S_{11} dip on resonance evidences that the resonator is overcoupled to the feedlines (Fig. 2a). The resonance frequency of the resistive resonator is v_0(Ag) $= 9.2118$ GHz while that of the superconducting one is v_0(Nb) $= 9.0775$ GHz, accordingly to the different ϵ_r of the two substrates. A well-defined transmission peak is observed in both cases (Fig. 2b). The Q-factor of the transmission resonance is calculated by means of the 3-dB rule. For the resistive
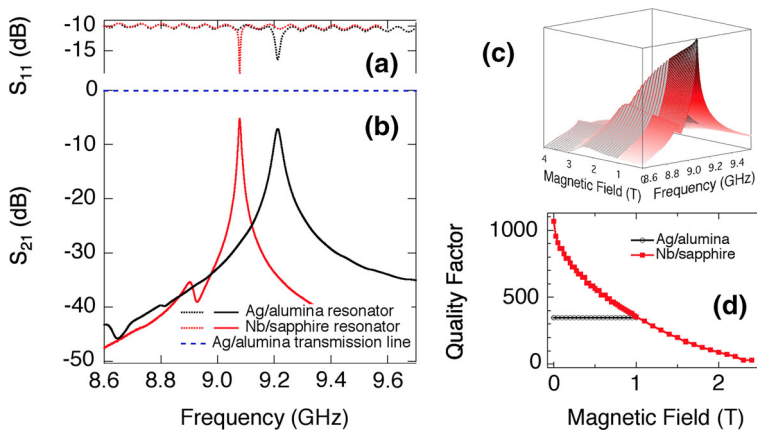

Fig. 2 Comparison between the characteristics of the Ag/alumina and Nb/sapphire resonators at $T = 2$ K. **a** Reflection spectra (*dotted lines*). The absolute value of S_{11} includes also the reflective background due to the coaxial line. **b** Transmission spectra (*solid lines*). The transmission spectrum of the broadband microstrip is shown by the *blue dashed line*. **c** Magnetic field dependence of the transmission spectrum measured for the Nb/sapphire resonator. **d** Q-vs.-B_0 curves extracted from the transmission spectra. The quality factor at zero field is 349 for the resistive resonator and 1068 for the superconducting one (color figure online)

resonators it was typically obtained in the range between 300 and 600 while for the Nb/sapphire resonator is $\sim 10^3$. Concerning the insertion loss (IL), we obtained IL = 7 dB for the resistive resonator and IL = 5 dB for the superconducting one (Fig. 2c). For comparison, the broadband transmission line (blue line) shows a flat response in this range and IL < 0.5 dB.

The transmission resonance of the Nb/sapphire resonator is strongly affected by an external magnetic field. Figure 2c shows a series of frequency spectra measured under applied field up to 2.5 T. The insertion loss rapidly increases with increasing B_0, thus the quality factor decreases, although for $B_0 < 1$ T it remains higher than the Q-factor shown by the resistive resonator (Fig. 2d). The resonance peak disappears in proximity to the dc upper critical field of the Nb film ($H_{c2} \sim 3$ T).

3 Continuous Wave EPR on Cr$_3$ Triangles

Since the resonance frequency is stable under applied field, the microwave absorption of the Cr$_3$ sample was evaluated by measuring the modulus of S_{21} at fixed frequency while sweeping B_0, in a similar way to continuous wave EPR spectroscopy. The EPR signal is directly obtained from the VNA, that is a valid alternative to the standard setup with modulation coil and lock-in detection. Millimeter-sized single crystals of molecular triangles of $Cr_3OPiv_6(H_2O)_3Piv$ were positioned directly above the central strip by means of a small amount of Apiezon N grease. The crystals have shape of hexagonal prisms and are indexed by X-ray diffractometry. The Cr$_3$ triangles lay parallel to the hexagonal face, hence with their perpendicular axis parallel to the c-axis of the crystal. We initially started with the single crystal oriented with $c||\mathbf{B_0}$ ($\theta = 0$) and we acquired the spectra with the crystal placed in different positions on the Ag/alumina resonator (Fig. 3). We observed an absorption dip at 0.335 T which becomes more intense as we move the
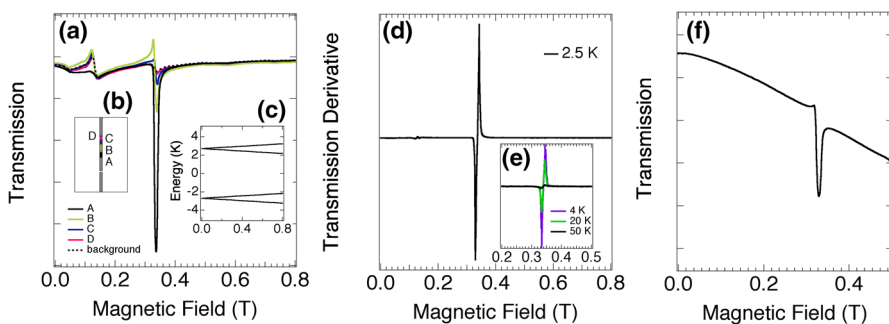

Fig. 3 **a** S_{21}-vs.-B_0 spectra measured with the Ag/alumina resonator loaded with a single crystal of Cr$_3$ ($T = 2.5$ K). As indicated in **b** the crystal is progressively shifted from the edge (D) to the center (A) of the central strip ($\theta = 0$). The continuous wave frequency is 9.215 GHz and the input power is +3 dBm. **c** Plot of the lowest lying energy levels of the Cr$_3$ crystal as a function of B_0 ($\theta = 0$). The ground state is constituted by two doublets separated by an energy gap of few K. **d** Numerical derivative of the transmission spectrum taken in the position A and **e** temperature dependence. **f** Continuous wave spectrum ($v = 9.064$ GHz) of a Cr$_3$ single crystal measured with the Nb/sapphire resonator

crystal from the edge to the center of the resonator. The latter corresponds to the position where $\mathbf{B_1}$ is maximum. This absorption dip thus can be assigned to the doublet transition of the Cr_3 ground state (Fig. 3c). Conversely, the dip at about 0.12 T is visible also in the spectrum of the bare resonator so it should be related to a small amount of magnetic impurities in the alumina substrate. Figure 3d shows the numerical derivative calculated from the signal in position A after the subtraction of the background. The spectrum shows the characteristic line shape of a doublet transition with $g_{\parallel} = hv/\mu_B B_{\parallel} = 1.97$ ($h = 6.6262 \times 10^{-34}$ J s, $\mu_B = 9.2741 \times 10^{-24}$ J T^{-1} and $v = 9.215$ GHz) and linewidth of 12 mT. The temperature dependence of the peak is shown in Fig. 3e with a progressive decrease of the EPR signal for increasing temperature.

Figure 4f shows the transmission spectrum measured for the Nb/sapphire resonator loaded with the Cr_3 crystal. In this case, the background signal has a constant slope due to the increase of IL under applied field (Fig. 2b). We also observed that the resonance frequency has some hysteresis, in particular for $B_0 < 0.1$ T. The absorption dip of the Cr_3 crystal is well visible at 0.329 T, that corresponds again to $g_{\parallel} = 1.97$.

To investigate the angular dependence of the doublet transition of Cr_3, we performed a series of measurements by orienting the c-axis of the crystal at different θ angles with respect to $\mathbf{B_0}$ (Fig. 4a). The crystal was manually rotated and θ was measured under the microscope by means of a goniometer. The derivative of the transmission signal of the resistive resonator is shown in the left panel for different θ angles. As θ increases, the transition moves toward higher field and becomes broader. For $\theta = 90°$ ($c \perp \mathbf{B_0}$) it is centered at about $B_{\perp} \approx 0.41$ T, thus the projection of the effective gyromagnetic factor in the plane of the ring is $g_{\perp} = hv/\mu_B B_{\perp} \approx 1.6$. Figure 4b displays the comparison with the signal measured for a polycrystalline sample of Cr_3. This spectrum shows multiple peaks due to the averaged contribution of different orientations.
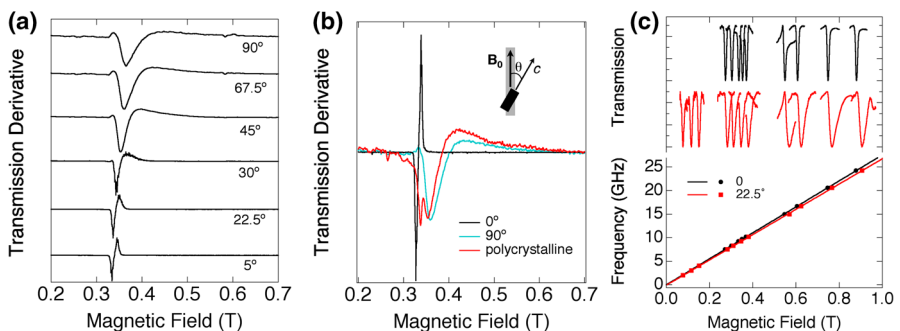

Fig. 4 **a** Derivative of the transmission spectra measured as a function of B_0 for different θ angles ($T = 2.5$ K). For each spectrum the intensity is normalized to its maximum value. **b** Comparison among the spectra taken at 0° and 90° and on a polycrystalline sample. **c** *Upper panel* absorption dips measured by means of the broadband microstrip for different frequencies and two orientations ($\theta = 0$, *black*; 22.5°, *red*). *Lower panel* plot of the microwave frequency as a function of the field position of the absorption dip (*markers*). *Solid lines* represent the best fit with a linear function (color figure online)

By means of the Ag/alumina broadband transmission line, we measured a series of continuous wave spectra for different frequencies in the range 2–25 GHz. Here the absorption signal is weaker with respect to the resonator, nevertheless the doublet transition of Cr_3 can be clearly identified. In the upper panel of Fig. 4c we show a series of absorption dips acquired for two orientations ($\theta = 0$ and 22.5°) and different frequencies. A linear dependence is obtained by plotting the frequency of excitation as a function of the field position of the absorption dip (lower panel of Fig. 4c). The curves are well fitted by means of $\nu = g\mu_B B/\hbar$, with $g = g_\parallel = 1.97$ for $\theta = 0$ (solid black line), and $g = \sqrt{g_\parallel^2 \sin^2\theta + g_\perp^2 \cos^2\theta}$ with $g_\perp = 1.6$ for $\theta = 22.5°$ (red line). These $g_\parallel$ and $g_\perp$ values are compatible to those obtained in Ref. [23] for a similar Cr_3 derivative and demonstrate that the frequency dependence of the resonance can be measured in this configuration at low temperature and sweeping magnetic field.

4 Conclusions

In conclusion, resistive and superconducting microstrips can be successfully employed to study the EPR transitions in single crystals of molecular nanomagnets. In the present study, we focused on Cr_3 molecular triangles and our results evidence the presence of anisotropic interactions, as shown for other variants of Cr_3 [22, 23].

In spite of higher Q in zero field, the magnetic field dependence of the superconducting properties poses serious limitation for the exploitation of Nb resonators for EPR spectroscopy in strong magnetic field: from the comparison of our resonators, for instance we found that at 1 T the quality factor of the Nb resonator is comparable to that of Ag.

The approach we used is simple and versatile and can be applied for other classes of materials or experimental configurations (e.g., parallel-mode EPR). Miniaturization of the microstrip for the investigation of very small samples could be achieved by using thin dielectric substrates, although the coplanar geometry is better indicated for this purpose. Thanks to their reduced dissipation and efficient microwave conversion, these devices are suitable for the installation on mK refrigerators and it will be also interesting to use them for pulsed EPR experiments at very low temperature.

References

1. J.A. Weil, J.R. Bolton, *Electron Paramagnetic Resonance*, 2nd edn. (Wiley, NewYork, 2008)
2. K.Y. Choi, Z. Wang, H. Nojiri, J. van Tol, P. Kumar, P. Lemmens, B.S. Bassil, U. Kortz, N.S. Dalal, Phys. Rev. Lett. **108**, 067206 (2012)

3. B. Johansson, S. Haraldson, L. Pettersson, O. Beckman, Rev. Sci. Instrum. **45**, 1445 (1974)
4. A. Torrezan, T. Mayer Alegre, G. Medeiros-Ribeiro. Rev. Sci. Instrum. **80**, 075111 (2009)
5. G. deLoubens, G. D. Chaves-O'Flynn, A. D. Kent, C. Ramsey, E. delBarco, C. Beedle, D. N. Hendrickson, J. Appl. Phys. **101**, 09E104 (2007)
6. J. Henderson, C. Ramsey, H. Quddusi, E. Del Barco, Rev. Sci. Instrum. **79**, 074704 (2008)
7. J.J. Henderson, C.M. Ramsey, E. del Barco, T.C. Stamatatos, G. Christou, Phys. Rev. B **78**, 214413 (2008)
8. O. Benninghof, H. Mohebbi, I. Taminiau, G. Miao, D. Cory, J. Magn. Reson. **230**, 84 (2013)
9. P. Bushev, A.K. Feofanov, H. Rotzinger, I. Protopopov, J.H. Cole, C.M. Wilson, G. Fischer, A. Lukashenko, A.V. Ustinov, Phys. Rev. B **84**, 060501 (2011)
10. H. Malissa, D. Schuster, A. Tyryshkin, A. Houck, S. Lyon, Rev. Sci. Instrum. **84**, 025116 (2013)
11. C. Clauss, D. Bothner, D. Koelle, R. Kleiner, L. Bogani, M. Scheffler, M. Dressel, Appl. Phys. Lett. **102**, 162601 (2013)
12. G. Boero, M. Bouterfas, C. Massin, F. Vincent, P.A. Besse, R.S. Popovic, A. Schweiger, Rev. Sci. Instrum. **74**, 4794 (2003)
13. R.S.R. Narkowicz, D. Suter, J. Magn. Reson. **175**, 275284 (2005)
14. R. Narkowicz, D. Suter, I. Niemeyer, Rev. Sci. Instrum. **79**, 084702 (2008)
15. Y. Twig, E. Suhovoy, A. Blank, Rev. Sci. Instrum. **81**, 104703 (2010)
16. G. Goglio, S. Pignard, A. Radulescu, L. Piraux, I. Huynen, D. Vanhoenacker, A. Vander Vorst, Appl. Phys. Lett. **75**, 1769 (1999)
17. F. Giesen, J. Podbielski, T. Korn, M. Steiner, A. VanStaa, D. Grundler, Appl. Phys. Lett. **86**, 112510 (2005)
18. Y. Liu, L. Chen, C. Tan, H. Liu, C. Ong, Rev. Sci. Instrum. **76**, 063911 (2005)
19. Z.L. Xiang, S. Ashhab, J.Q. You, F. Nori, Rev. Mod. Phys. **85**, 623 (2013)
20. Y. Simonov, P. Bourosh, G. Timco, S. Grebenco, S. Mazus, C. Indrichan, N. Gerbeleu, Chem. Bull. Polytechnic Univ. Timisoara Romania **43**, 128 (1998)
21. K. Gupta, R. Garg, I. Bahl, P. Bhartia, *Microstrip Lines and Slotlines* (ArtechHouse, Boston, 1996)
22. A. Vlachos, V. Psycharis, C.R. Raptopoulou, N. Lalioti, Y. Sanakis, G. Diamantopoulos, M. Fardis, M. Karayanni, G. Papavassiliou, A. Terzis, Inorg. Chim. Acta **357**, 3162 (2004)
23. A. Figuerola, V. Tangoulis, J. Ribas, H. Hartl, I. Brudgam, M. Maestro, C. Diaz, Inorg. Chem. **46**, 11017 (2007)